数理解析研究所講究録
第 332 巻 1978 年 11-36

A PICTURE BOOK OF STOCHASTICITY*

Joseph Ford
School of Physics, Georgia Institute of Technology
Atlanta, Georgia 30318

ABSTRACT

Once upon a time, not so long ago, the Hamiltonian $H(Q,P) = H_0(P) + \varepsilon V(Q,P)$ was regarded as a very unpredictable fellow -- sometimes nice and integrable but more often violently stochastic. This is the story of how he got that way and why it matters. It all involves resonances in his personality and how they interact, so lets begin with them ...

INTRODUCTION

At this Christmas season conference on non-linear dynamics, it is perhaps quite appropriate to introduce the following pictorial review with the above fable-like title and abstract. But the analogy lies much deeper; for the story we present here, treating non-linear resonances as the source of chaotic trajectory behavior in Hamiltonian system, is a highly valuable but nonetheless intuitive "fable" which will eventually be replaced by a more rigorous, if less picturesque, general theory. Even so, this "fable" will likely serve as a convenient introduction to an incredibly complex subject for many years to come. Various versions[1] of this story have appeared frequently in the recent literature, and many in this audience will be quite familiar with it. For them, it is hoped that this retelling of the tale contains at least a few interesting deviations from time to time.

HAMILTONIAN SYSTEMS

In order to introduce the notation in our most general Hamiltonian systems, let us begin with the oscillator system.

$$H = \frac{1}{2}\sum_{k=1}^{N}(P_k^2 + \omega_k^2 Q_k^2) + V_3(Q,P) + V_4(Q,P) + \ldots, \quad (1)$$

where the Q_k and P_k denote coordinates and momenta respectively, where $\omega_k > 0$ are the positive frequencies of the harmonic approximation, and where V_3, V_4, ... denote cubic, quartic, ... polynominals in the Q_k and P_k. We now canonically change variables from the "rectangular" (Q_k,P_k) coordinates to the "polar" coordinates (ϕ_k, J_k) via

*This work supported in part by the National Science Foundation

$$Q_k = (2J_k/\omega_k)^{1/2} \cos \phi_k, \quad P_k = -(2J_k\omega_k)^{1/2} \sin \phi_k. \tag{2}$$

In these "polar" coordinates, Hamiltonian (1) reads

$$H = H_0(J_1,\ldots,J_N) + \varepsilon\, V(J_1,\ldots,\phi_N), \tag{3}$$

where all the pure J-terms are included in H_0, where V involves only angle dependent terms, and where ε is a perturbation parameter introduced so that we may regard V as a perturbation on the obviously solvable (integrable) H_0. Independent of its origin, we regard Eq. (3) as specifying our most general conservative Hamiltonian system. Generalizing slightly, we permit V to depend periodically on the time variable $\tau = \Omega t + \tau_0$ and write

$$H = H_0(J_1,\ldots,J_N) + \varepsilon V(J_1,\ldots,\phi_N, \tau). \tag{4}$$

Expanding Hamiltonian (4) in a "double" Fourier series, we may write

$$H = H_0(J_1,\ldots,J_N) + \varepsilon \sum V_{mn}(J)\cos\,(m\cdot\phi+n\tau), \tag{5}$$

where $m\cdot\phi = \sum m_k\phi_k$. We shall regard Hamiltonian (5) as our most general Hamiltonian system. Equation (5) has several virtues:

1. H_0 is obviously integrable,
2. The resonant terms are "obvious",
3. H_0 plus any single angle dependent term is integrable.

The equations of motion for the unperturbed Hamiltonian H_0 read

$$\dot{J}_k = 0 \quad \text{and} \quad \dot{\phi}_k = \partial H_0/\partial J_k \equiv \omega_k(J), \tag{6}$$

where the dot superscript denotes time derivative. Equations (6) have the immediate solution

$$J_k = J_{k0} \quad \text{and} \quad \phi_k = \omega_k(J)t + \phi_{k0}, \tag{7}$$

where J_{k0} and ϕ_{k0} denote initial values and where, in general, $\omega_k = \omega_k(J_1,\ldots,J_N)$. We have thus shown that H_0 is integrable (solvable) by the simple device of directly integrating its equations of motion. More generally, any Hamiltonian which can be canonically transformed by an analytic, single-valued change of

variables to read $H = H_0(J_1,\ldots,J_N)$ is said to be integrable.[2] Such a transformation will exist when a Hamiltonian $H(Q_1,\ldots P_N)$ has N independent, analytic, single-valued constants of the motion. Trajectories for such integrable systems must lie on the smooth, N-dimensional surfaces defined by the constant J_k. For bounded motion, these surfaces are tori.[2] We may regard the J_k as specifying the constant "radii" of the tori with the ϕ_k providing the angular positions. In Fig. 1, we show a cross-sectional view of a torus for the case N = 2. Quite generally for any integrable system, its trajectories lie on one or another of a set of nested tori with each torus bearing quasi-periodic (or strictly periodic) motion having the constant frequencies $\omega_k = \omega_k(J_1,\ldots J_N)$.

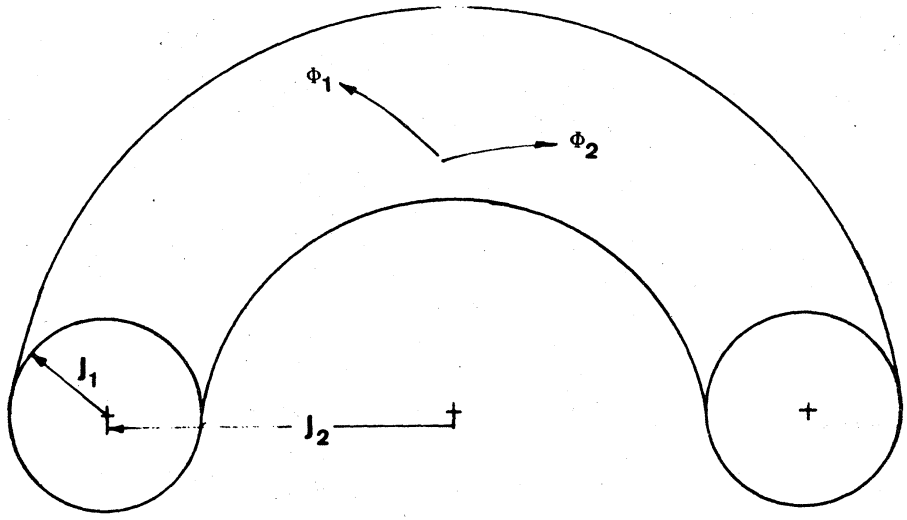

Fig. 1. A cross-sectional view of a two-dimensional torus or doughnut. The variables are those which appear in eq. (7) when N = 2.

Whenever one or another of the perturbing terms in Eq. (5) "drives" the H_0-motion at one of the natural frequencies occurring on one of its tori, then one expects a resonant response in which the affected trajectory departs the confines of its H_0-torus. But how do we recognize such a resonant term in Eq. (5)? Let us consider a single perturbing term and write

$$H = H_0(J) + \varepsilon\, V_{mn}(J) \cos\,(m\cdot\phi+n\tau) + \ldots \quad . \qquad (8)$$

Then the equations of motion are

$$\dot{J}_k = \varepsilon\, m_k\, V_{mn}(J) \sin\,(m\cdot\phi+n\tau), \qquad (9a)$$

$$\dot{\phi}_k = \omega_k + \varepsilon(\partial V_{mn}/\partial J_k) \cos(m\cdot\phi+n\tau) . \qquad (9b)$$

When ε is small, we may use $J_k = J_{k0}$ and $\phi_k = \omega_k t + \phi_{k0}$ on the right hand side of Eq. (9a) to obtain

$$J_k = J_{k0} - \frac{\varepsilon m_k V_{mn} \cos(m\cdot\phi+n\tau)}{[m\cdot\omega(J)+n\Omega]} \qquad (10)$$

valid to first order in ε. Thus, we immediately see that a given term $\cos(m\cdot\phi+n\tau)$ is resonant at first order in ε provided that

$$[m\cdot\omega(J)+n\Omega] \lesssim \varepsilon \qquad (11)$$

for some values of J, where $\omega(J) = \partial H_0/\partial J$. In particular, a term $\cos(m\cdot\phi+n\tau)$ for which $n > 0$ and all $m_k > 0$ can never be resonant, at least to first order in ε.

Finally, if the sum in Hamiltonian (5) is replaced by any single one if its terms, then Hamiltonian (5) becomes integrable as we show via several examples in the following.

RESONANCE IN SIMPLE ONE DEGREE OF FREEDOM SYSTEMS

To see what all this looks like for a simple example, let us begin with the driven harmonic oscillator described by

$$\ddot{q} = -\omega_0^2 q + \varepsilon A\cos\tau , \qquad (12)$$

where $\tau = \Omega t + \tau_0$. The associated Hamiltonian is

$$H = (1/2)(p^2 + \omega_0^2 q^2) - \varepsilon A q \cos\tau . \qquad (13)$$

Then using $q = (2J/\omega_0)^{1/2}\cos\phi$ and $p = -(2J\omega_0)^{1/2}\cos\phi$, we find

$$H = \omega_0 J - \frac{\varepsilon A}{2}\left(\frac{2J}{\omega_0}\right)^{1/2}[\cos(\phi-\tau) + \cos(\phi+\tau)] , \qquad (14)$$

where here $H_0 = \omega_0 J$ Let us now note that the driven solution of Eq. (12) [or Hamiltonian (14)] may be written

$$\frac{\varepsilon A\cos\tau}{\omega_0^2 - \Omega^2} = \frac{\varepsilon A}{2\omega_0}\frac{\cos\tau}{(\omega_0 - \Omega)} + \frac{\varepsilon A}{2\omega_0}\frac{\cos\tau}{(\omega_0 + \Omega)} \qquad (15)$$

Moreover, it is straightforward to show that $[\varepsilon A\cos\tau/2\omega_0(\omega_0-\Omega)]$ is the driven solution of the harmonic (linear) oscillator Hamil-

tonian

$$H = \omega_0 J - \frac{\varepsilon A}{2}\left(\frac{2J}{\omega_0}\right)^{1/2} \cos(\phi-\tau) \ . \qquad (16)$$

while $[\varepsilon A \cos \tau/2\omega_0(\omega_0+\Omega)]$ is the driven solution for the harmonic

$$H = \omega_0 J - \frac{\varepsilon A}{2}\left(\frac{2J}{\omega_0}\right)^{1/2} \cos(\phi+\tau) \ . \qquad (17)$$

Thus, as anticipated, Hamiltonian (16) retains all the essential resonant behavior of Hamiltonian (14).

Let us now slightly modify Hamiltonian (16) to obtain the non-linear oscillator Hamiltonian

$$H = \omega_0 J + \alpha J^2 - \frac{\varepsilon A}{2}\left(\frac{2J}{\omega_0}\right)^{1/2} \cos(\phi-\tau) \ , \qquad (18)$$

where now $\omega(J) = \partial H_0/\partial J = (\omega_0 + 2\alpha J)$ depends on J when $\alpha \neq 0$. Then, by introducing the time-dependent, canonical change of variables $J = J$ and $\Theta = \phi-\tau$, we may obtain the time-independent Hamiltonian

$$H = (\omega_0-\Omega)J + \alpha J^2 - \frac{\varepsilon A}{2}\left(\frac{2J}{\omega_0}\right)^{1/2} \cos\Theta \ . \qquad (19)$$

In Eq. (19), H is a constant of the motion and we may graph its trajectories just as we graph the elliptical orbits for $H = (1/2) \times (p^2 + \omega_0^2 q^2)$. In this way, we may easily visualize certain differences between linear and non-linear resonances.

When $\alpha = 0$, we typically obtain the graph shown in Fig. 2, where $Q = (2J/\omega_0)^{1/2} \cos\Theta$ and $P = -(2J\omega_0)^{1/2} \sin\Theta$. Here we note that the driving resonance displaces the unperturbed $\varepsilon = 0$ orbits laterally along the Q-axis. The equilibrium point on the Q-axis corresponds to the periodic driven solution of Eq. (15). As Ω tends to ω_0, this equilibrium point tends to infinity. Thus at precise resonance $\Omega = \omega_0$, all the orbits diverge as vertical straight lines to infinity. Moreover even near resonance $\Omega \simeq \omega_0$, the orbit initially passing through the origin $J(0) = 0$ $[Q(0) = P(0) = 0]$ is unstable and departs arbitrarily far from the origin as Ω tends toward ω_0.

For $\alpha \neq 0$, the non-linear dependence of ω on J, given by $\omega = \omega_0 + 2\alpha J$, stabilizes this resonance, and the orbit passing

through $J(0) = 0$, for example, is always bounded even at $\Omega = \omega_0$.

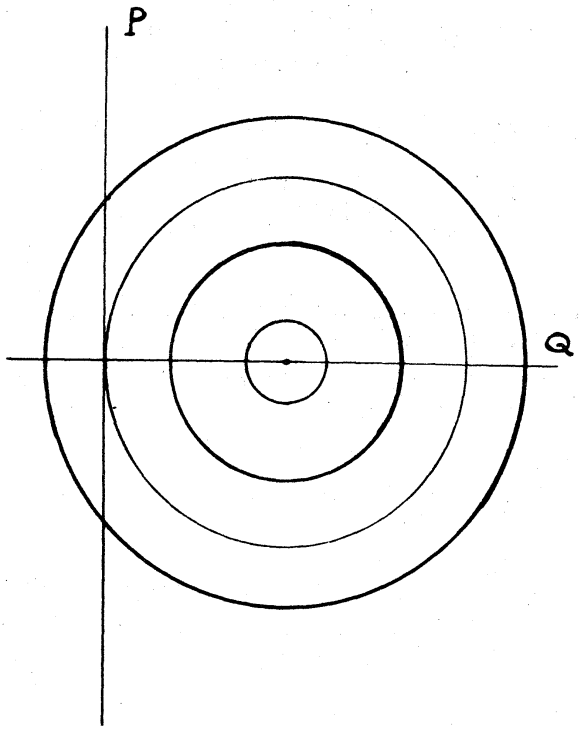

Fig. 2. A graph of orbits for Hamiltonian (19) with $\alpha = 0$. Here $\Omega \neq \omega_0$.

Indeed, set $\Omega = \omega_0$ in Eq. (19). Then for $J(0) = 0$, we have that $H \equiv 0$. Solving Eq. (19) for J then yields the bounded orbit

$$J^3 = \frac{\epsilon}{4\alpha}\left(\frac{2}{\omega_0}\right)[1 + \cos 2\Theta] \ , \qquad (20)$$

where we have discarded the solution $J = 0$. But the dependence of ω on J has another equally significant effect, for now we always have a resonant J-value near which $\omega(J) \simeq \Omega$. In particular when $\Omega \neq \omega_0$ and $|\Omega - \omega_0| >> 1$, we have the picture shown in Fig. 3. Here, we note that the non-linearity has introduced two new equilibrium points on the Q-axis (one stable and one unstable) in addition to the "linear" equilibrium point near the origin. Had α been zero here, we would have had only ovals essentially centered on the origin; but for $\alpha \neq 0$, we find the bounded non-linear resonant zone shown in Fig. 3 which has a finite ΔJ width. Indeed, as α decreases or ϵ increases, this width can become rather large.

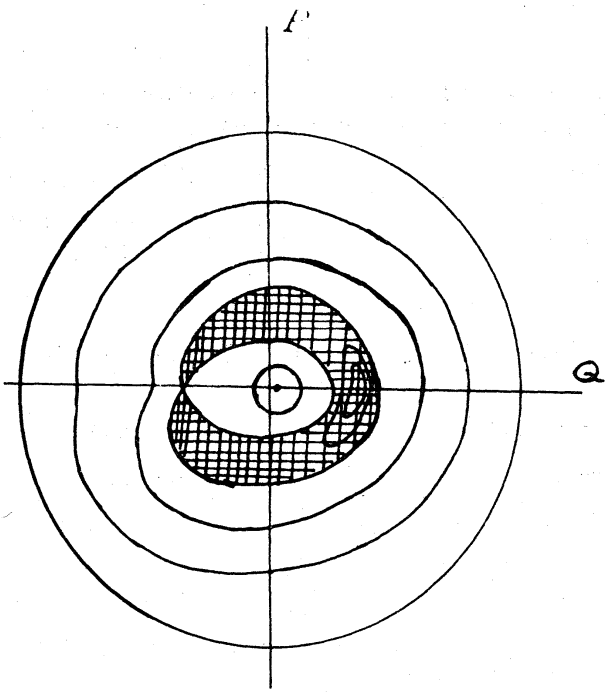

Fig. 3. A graph of orbits for Hamiltonian (19) with $\alpha \neq 0$ and $|\Omega-\omega_0| \gg 1$. The zone of non-linear resonance is cross-hatched.

RESONANCE IN SIMPLE, CONSERVATIVE TWO DEGREES OF FREEDOM SYSTEM

In order to obtain some typical pictures of resonant zones for conservative systems with two degrees of freedom, let us first consider the system

$$H = J_1+J_2-J_1^2-3\,J_1J_2+J_2^2+\varepsilon\,J_1J_2\cos 2(\phi_1-\phi_2), \quad (21)$$

where $H_0 = J_1+J_2-J_1^2-3\,J_1J_2+J_2^2$. Recall now that the H_0 orbits lie on two-dimensional tori, one of which is drawn in Fig. 1. Each torus bears orbits having frequencies given by $\omega_1 = 1-2\,J_1-3\,J_3$ and $\omega_2 = 1-3\,J_1+2\,J_1$. We thus expect the small perturbation $\cos(2\phi_1-2\phi_2)$ to resonantly distort a zone of unperturbed tori "centered" about the torus having $\omega_1(J_1,J_2) = \omega_2(J_1,J_2)$.

We now note that Hamiltonian (21), itself a constant of the motion, has the additional constant $I = J_1+J_2$. Thus Hamiltonian (21) is integrable, yielding motion lying on perturbed tori. We thus wish to determine here the distortion of the $\varepsilon = 0$ tori when $\varepsilon \neq 0$. If we use $I = J_1+J_2$ to eliminate J_1 from Eq. (21), we obtain

$$H = I-I^2+[2-\varepsilon\cos 2(\phi_1-\phi_2)]J_2^2-[1-\varepsilon\cos 2(\phi_1-\phi_2)]IJ_2, \quad (22)$$

which defines the two-dimensional perturbed tori lying in the three-space (J_2,ϕ_1,ϕ_2). If we now set $\phi_1 = 3\pi/2$ in Eq. (22), we obtain the intersection of the tori with the plane $\phi_1 = 3\pi/2$. In short, we obtain a two-dimensional, cross-sectional view of the perturbed tori. In the (J_2,ϕ_2) plane, the cross-sectional curves are given by

$$H = I - I^2 + [2+\varepsilon \cos 2\phi_2]J_2^2 - [1+\varepsilon \cos 2\phi_2]IJ_2 . \qquad (23)$$

In Fig. 4, we present a typical cross-sectional view of the perturbed tori, where $Q_2 = (2J_2)^{1/2} \cos \phi_2$ and $P_2 = -(2J_2)^{1/2} \sin \phi_2$. Here we note that the unperturbed $\varepsilon = 0$ tori (given by $J_2 =$ constant) are only slightly distorted except in the crescent shaped resonant zones for which $\omega_1(J_1,J_2) \approx \omega_2(J_1,J_2)$. Also, let us note that the positions and widths of these resonant zones vary as ε or the energy $H = E$ change.

Next, let us consider the integrable resonance

$$H = J_1 + J_2 - J_1^2 - 3J_1J_2 + J_2^2 + \varepsilon J_1J_2^{3/2} \cos (2\phi_1 - 3\phi_2) \qquad (24)$$

which has the additional constant $I = 3J_1 + 2J_2$. Note that H_0 is the same for both Eq. (21) and Eq. (24). Equation (21) perturbs H_0 with a so-called 2-2 resonance while Eq. (24) involves the 2-3 resonance. We expect $\cos (2\phi_1 - 3\phi_2)$ to distort the unperturbed $\varepsilon = 0$ tori bearing frequencies $2\omega_1(J_1,J_2) \approx 3\omega_2(J_1,J_2)$. The equation for the cross-sectional curves of perturbed tori here reads

$$H = \frac{I}{3} - \frac{I^2}{9} + \left(\frac{1}{3} - \frac{5}{9} I\right)J_2 + \frac{23}{9} J_2^2 + \varepsilon\left[\frac{2}{3} J_2^{5/2} - \left(\frac{I}{3}\right)J_2^{3/2}\right] \cos 3\phi_2 . \qquad (25)$$

Typical curves generated by Eq. (25) are shown in Fig. 5.

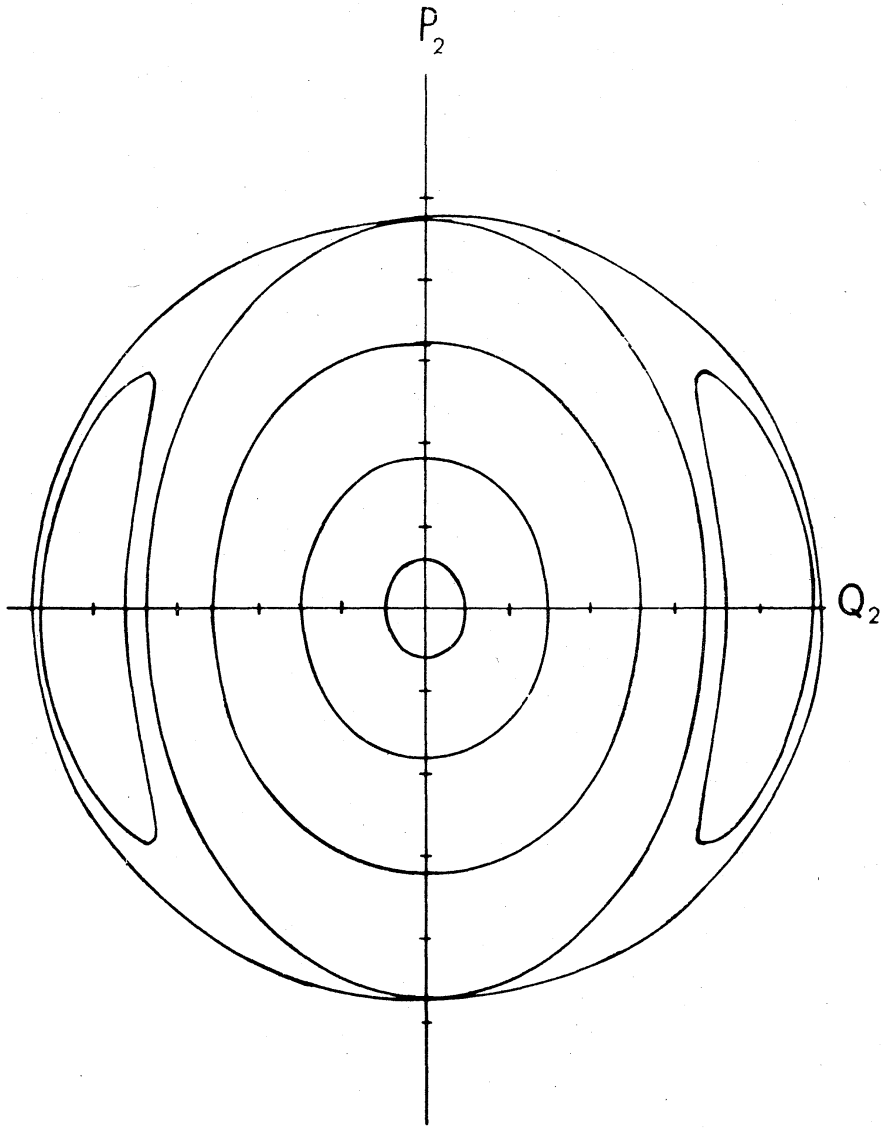

Fig. 4. A cross-sectional view of the perturbed tori for the integrable Hamiltonian (21). The crescent shaped regions are the resonant regions.

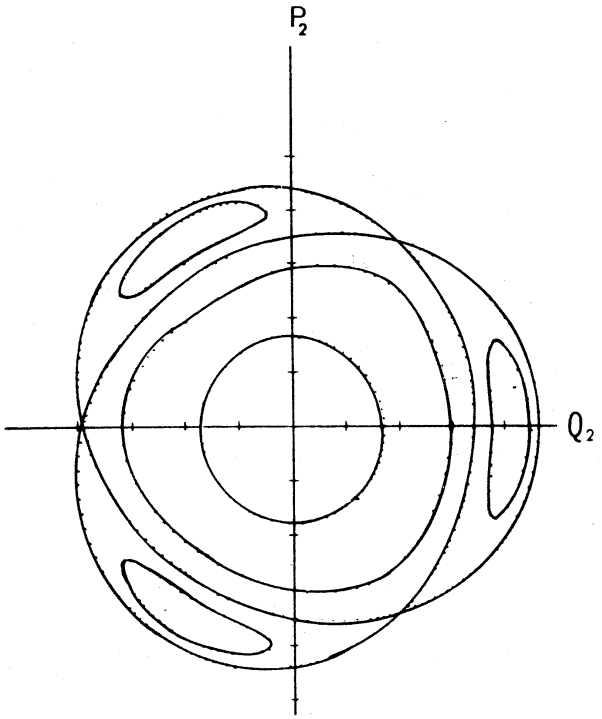

Fig. 5. A cross-sectional view of the perturbed tori for Hamiltonian (24). The 2-3 resonant zone appears as the triple crescent region.

It must be noted here that the unperturbed $2\omega_1 = 3\omega_2$ torus does not occur for $E < 0.16$; thus, Fig. 5 is for an energy above this value.

Finally let us note that we could have obtained Figs. 4 and 5 by direct numerical integration of the equations of motion. Here one would merely integrate orbits and plot those (J_2,ϕ_2) values for orbit points at which $\phi_1 = 3\pi/2$.

RESONANCE OVERLAP AND STOCHASTIC BEHAVIOR

We now inquire about the effect on the H_0 motion of the previous section when both the 2-2 and the 2-3 resonances act simultaneously. In particular, we ask what occurs when the individual resonant zones as computed in the previous section are predicted to overlap. Thus, we now consider

$$H = J_1+J_2-J_1^2-3J_1J_2+J_2^2+\varepsilon J_1J_2\cos(2\phi_1-2\phi_2)$$

$$+ \varepsilon J_1J_2^{3/2}\cos(2\phi_1-3\phi_2)\ . \qquad (26)$$

Using Eqs. (23) and (25) of the previous section, we first obtain Fig. 6 which graphs the positive Q_2-axis intercept of the inner edge of the 2-2 resonant zone and the outer edge of the 2-3 resonant zone as a function of energy $H = E$ for fixed $\varepsilon = 0.02$. Overlap is predicted to occur at $E = 0.2095$. Using direct numerical

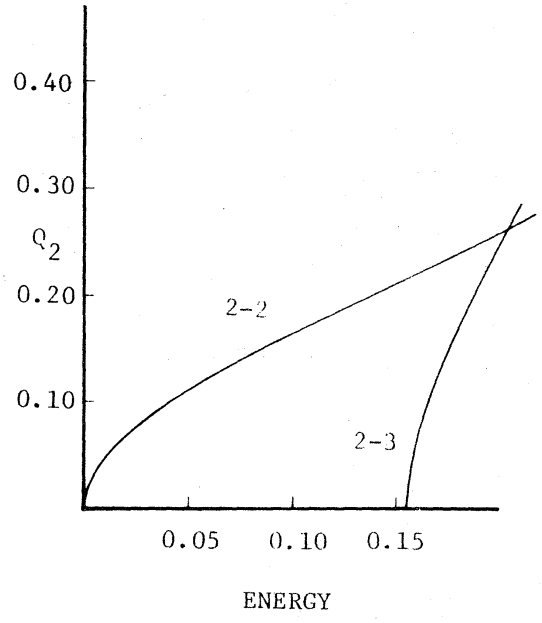

Fig. 6. Q_2-axis intercepts of the inner edge of the 2-2 zone and the outer edge of the 2-3 zone as a function of energy.

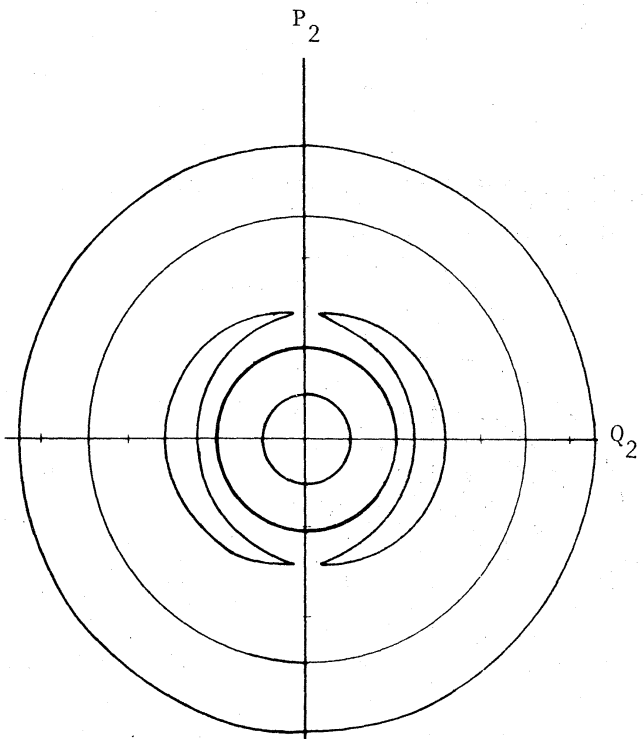

Fig. 7. Directly integrated cross-sectional view of Hamiltonian (26) at energy E = 0.056 .

integration of Hamiltonian (26) at energy E ≈ 0.056, we obtain the (Q_2,P_2)-plane cross-sectional view shown in Fig. 7. Here the 2-3 resonance zone has not yet appeared. In Fig. 8, we show the directly integrated curves at energy E = 0.18 where now the well separated 2-2 and 2-3 zones both appear. In Fig. 9, we

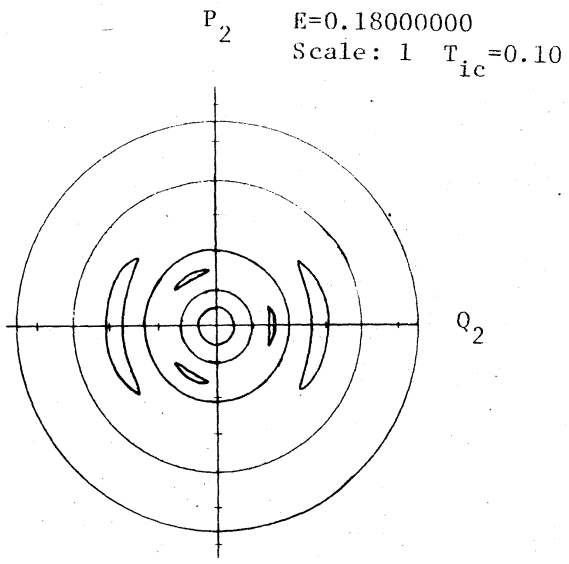

Fig. 8 A (Q_2,P_2)-plane cross-sectional view for Hamiltonian (26) at energy E = 0.18.

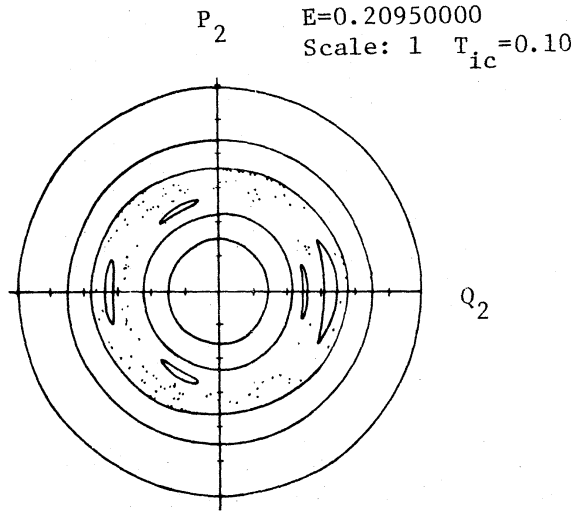

Fig. 9 The (Q_2,P_2)-plane at the energy predicted to yield resonance overlap.

show the appearance of the (Q_2,P_2)-plane cross-section at the predicted overlap energy of E = 0.2095. Here the chaotic set of dots was generated by a single orbit. The region of "overlap" thus appears to give rise to a so-called stochastic zone in which orbits are extremely erratic.

In order to gain further insight into the source of this chaotic region, let us examine Fig. 10 which shows the (Q_2,P_2)-plane at the slightly lower energy E = 0.20. Here we observe a previously unexpected narrow resonant zone containing five crescent regions which lie between the 2-2 and the 2-3 zones; in addition, a very narrow resonant zone (not shown) containing seven crescents has also been detected. These secondary resonances arise because of the interaction between the two explicitly appearing primary resonances in Hamiltonian (26). Indeed canonical

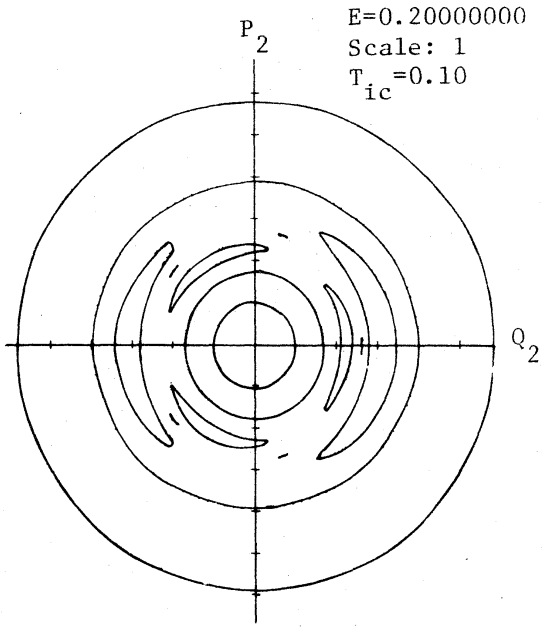

Fig. 10. At energy E = 0.20 an additional secondary resonant zone containing five narrow crescents appears between the primary 2-2 and 2-3 zones.

perturbation theory[1] may be used to show that a host of secondary and higher order resonances occur in the "overlap" region. As a consequence, orbits in this region move under the influence of many competing resonances and therefore develop acute vertigo, wandering aimlessly through phase space. Moreover as the energy increases, the size of this chaotic stochastic region increases, in many cases completely filling the allowed phase space.

If one initially starts two orbits very close together in a curve bearing region of the (Q_2,P_2)-plane, one obtains the typical linear separation shown in Fig. 11. On the other hand, two initially close orbits started in the chaotic region separate exponentially with a typical case being shown in Fig. 12. It is this sensitive exponential "forgetting" of initial conditions that leads one to label the chaotic regions as stochastic since here the final system state depends as sensitively on initial conditions as does a dice roll. Moreover, computer experiments indicate that the chaotic regions contain a dense set of unstable periodic orbits; thus one may regard the aperiodic orbits as stochastically diffusing among the dense set of scattering orbits. Further insights into the nature of these stochastic regions will be provided in later sections.

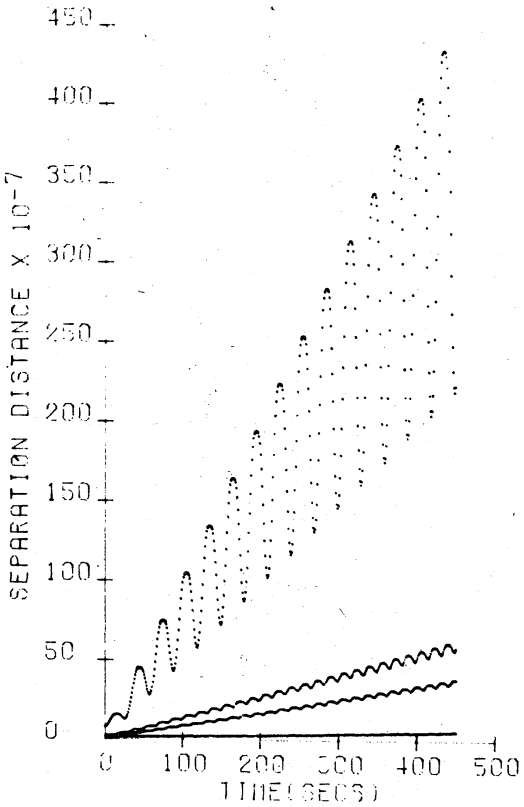

Fig. 11. This figure shows the growth of separation distance between two trajectories initially started about 10^{-7} apart in the full sphase space. Separation distance versus time is plotted for four distinct orbit-pairs. Each orbit-pair starts in a smooth level-curve region and the linear growth of separation distance with time is apparent.

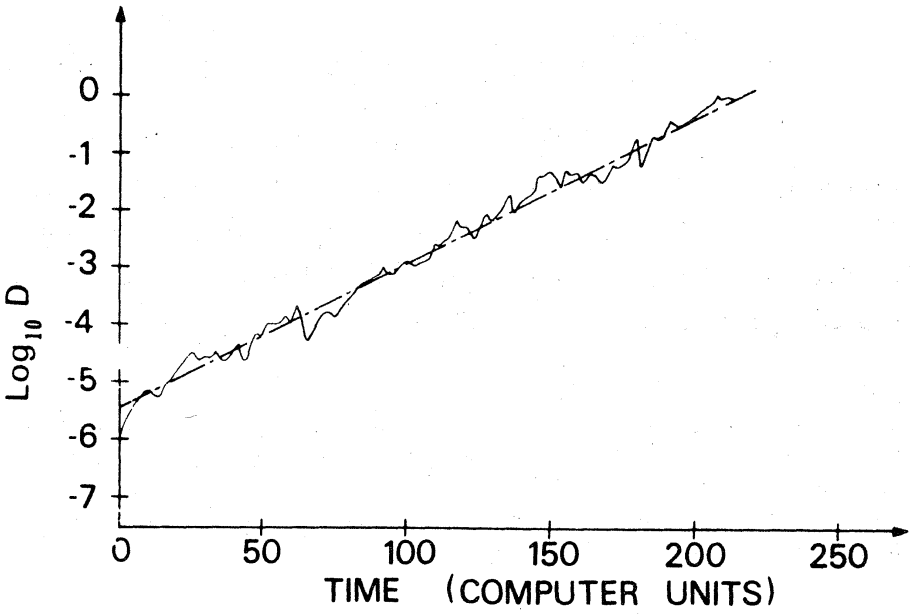

Fig. 12. Graph showing a typical curve of exponential growth in separation distance. Here, a curve of $\log_{10}D$ vs. time is plotted.

THE CHIRIKOV RESONANCE OVERLAP CRITERION

In the last two sections, we have illustrated that one may obtain an estimate of the critical parameter values at which a macroscopically visible stochastic zone first appears by computing the conditions for primary resonance overlap. Here, each primary resonance zone is computed as if that resonance were acting alone. In this section we discuss Chirikov's procedure[3] for computing this estimate. In particular, we shall illustrate his method as applied to one specific example system.

First, Chirikov computes the location and resonant width of an isolated resonance. As an example, let us consider the one degree of freedom driven oscillator

$$H = H_0(J) + \varepsilon\, V(J) \cos(\Theta - \tau) , \qquad (27)$$

where $\tau = \Omega t + \tau_0$. The J-value J_r at the center of the resonant zone is determined using

$$\omega(J_r) = \partial H_0/\partial J \Big|_{J=J_r} = \Omega . \qquad (28)$$

Let us now introduce the time-dependent canonical change of variables $P = J - J_r$ and $\psi = \Theta - \tau$. Hamiltonian (27) then becomes

$$H = \frac{\omega'(J_r)}{2} P^2 + \varepsilon V(J_r) \cos \psi, \qquad (29)$$

where we have expanded $H_0(J_r+P)$ in powers of P retaining terms only through order P^2, where we have neglected $H_0(J_r)$, where we have retained only the lowest order term $V(J_r)$ in the expansion for $V(J_r+P)$, where the term linear in P vanishes since $\omega(J_r) = \Omega$, and where $\omega'(J_r) = \partial\omega/\partial J\Big|_{J=J_r}$.

Hamiltonian (29) has placed its origin at the "center" of the resonance zone resulting in what Chirikov terms the pendulum approximation since Eq. (29) is formally identical to a simple pendulum Hamiltonian. Chirikov now assumes that Hamiltonian (29) is valid out to the edge of the resonance zone. The phase plane diagram is shown in Fig. 13.

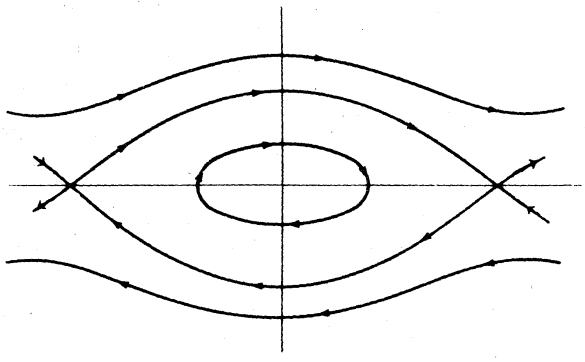

Fig. 13. The phase plane for Hamiltonian (29).

The pendulum resonant zone is bounded by the so-called separatrix curve passing through the unstable equilibrium points at $\psi = 0, \pi$ On the separatrix $H = \varepsilon V$, its value at $\psi = 0$. Thus, on the separatrix, we have

$$\omega' P^2/2 = \varepsilon V(1 - \cos \psi) = 2\varepsilon V \sin^2(\psi/2), \qquad (30a)$$

or

$$P_s = \pm 2(\varepsilon V/\omega')^{1/2} \sin(\psi/2). \qquad (30b)$$

In original variables, the value of J on the separatrix curve is

$$J = J_r \pm (\Delta J)_r \sin[(\Theta-\tau)/2], \qquad (31)$$

where the resonance half-width $(\Delta J)_r$ is given by

$$(\Delta J)_r = 2\,[\varepsilon V(J_r)/\omega'(J_r)]^{1/2}. \qquad (32)$$

Chirikov now further approximates by taking the resonance half-width in frequency $(\Delta\omega)_r$ to be given by

$$(\Delta\omega)_r = \omega'(J_r)\ (\Delta J)_r, \qquad (32a)$$

or

$$(\Delta\omega)_r = 2\,[\varepsilon\omega'(J_r)V(J_r)]^{1/2} \qquad (32b)$$

Equation (32b) is Chirikov's estimate for the resonant half-width in terms of the frequency ω and it is valid for Hamiltonian (27).

Let us now apply these formulas to the Hamiltonian

$$H = AJ^{4/3} - (\varepsilon/2)(3\beta J)^{1/3}\,[\cos\,(\Theta-\tau_1) + \cos\,(\Theta-\tau_2)], \qquad (33)$$

containing two explicit, primary driving resonances. Here A and β are constants. Now let Ω denote either Ω_1 or Ω_2. Then the pendulum approximation for either resonance acting alone yields a resonance centered at

$$J_r = \Omega^3/3\beta^4\ , \qquad (34)$$

with an ω half-width given by

$$(\Delta\omega)_r = \beta^{3/2}\ (2\varepsilon/\Omega)^{1/2}\ . \qquad (35)$$

Following Chirikov, we now define $\Delta\Omega \equiv |\Omega_1-\Omega_2|$ and we assume that $\Delta\Omega \ll \Omega_1$. In essence we are assuming that Ω_1 is close to but not identical with Ω_2. In terms of frequencies the two resonances are centered at $\Omega_1 = \omega(J_{r1})$ and $\Omega_2 = \omega(J_{r2})$; moreover the two resonant widths are approximately equal. Thus , the independent resonant zones will touch when

$$2(\Delta\omega)_r \approx \Delta\Omega, \qquad (36)$$

where $(\Delta\omega)_r$ is given by Eq. (35). Equation (36) is Chirikov's overlap criterion. Putting Eq. (35) into Eq. (36), we find

$$\frac{\Delta\Omega}{2} \approx \beta^{3/2}\ (2\varepsilon/\Omega)^{1/2}, \qquad (37)$$

where the Ω on the right is set equal to $(\Omega_1+\Omega_2)/2$. Equation (37) then predicts a critical ε value ε_c given by

$$\varepsilon_c \approx \Omega(\Delta\Omega)/8\beta^3. \tag{38}$$

For $\varepsilon \geq \varepsilon_c$, we expect that Hamiltonian (33) has a stochastic zone.

Chirikov now numerically integrates the equations of motion using $\Omega_1 = 0.217$, $\Omega_2 = 0.251$, $\Omega = 0.234$, $(3\beta J)_0^{1/3} = 0.276$, $\beta = 0.8472$, and $A = (3\beta/2\sqrt{2})^{4/3}$. Equation (38) yields $\varepsilon_c \cong 5.76 \times 10^{-5}$, while the numerical experiments described below yield $\varepsilon_c \approx 2.55 \times 10^{-5}$.

As he numerically integrates an orbit, Chirikov calculates what he calls a diffusion coefficient given by

$$D_n = \overline{[(\Delta\bar{H})^2/\Delta t]}. \tag{39}$$

Here, the total integration interval t is divided into many sub-intervals (Δt_n). The time varying total energy H is time averaged over each (Δt_n) sub-interval to yield $\bar{H}$. $\Delta\bar{H}$ is then the difference in $\bar{H}$ between any two sub-intervals (Δt_n) separated by a time interval Δt. The final average in Eq. (39) then involves averaging $[(\Delta\bar{H})^2/\Delta t]$ over all possible pairs of sub-intervals. For $\varepsilon < \varepsilon_c$, all orbits should yield D_n values which tend to zero as the total time interval t becomes large. On the other hand, for $\varepsilon \gtrsim \varepsilon_c$, an orbit started in the chaotic zone would be expected to yield a non-zero D_n due to an expected "random walk" of $\bar{H}$. In essence, Chirikov anticipates a fast exponential separation of the phase ψ for a group of initially close orbits followed by a much slower "random phase" diffusion of $\bar{H}$ itself. We shall make this "random walk" type behavior more transparent using some simple models which we discuss later. In any event, a graph of Chirikov's results is sketched in Fig. 14. Here one notes, as anticipated, an increase in D_n by many powers of ten as ε increases through ε_c.

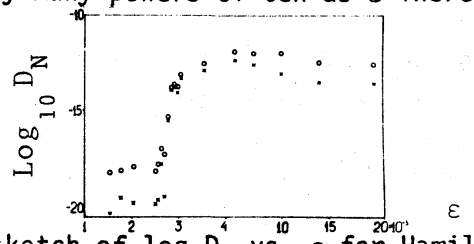

Fig. 14. A sketch of log D_n vs. ε for Hamiltonian (33).

THE BAKER'S TRANSFORMATION

We may illustrate the random walk character of the stochastic zones using a simple, rigorously ergodic[2] area preserving mapping of the unit square upon itself. Here the unit square is stretched

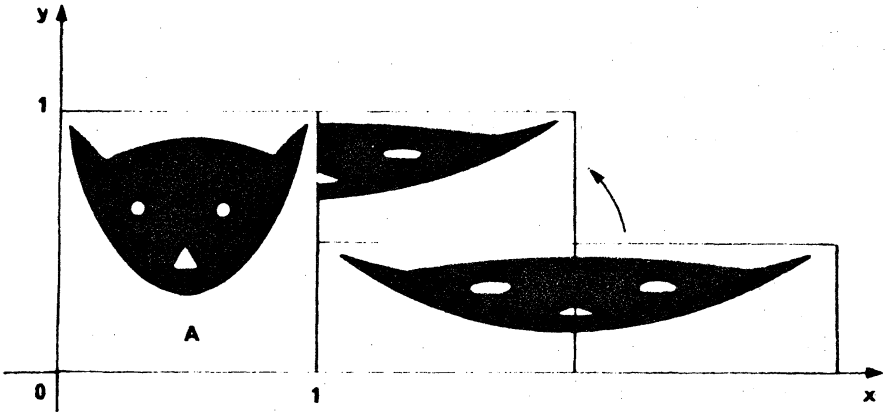

Fig. 15. A drawing of the baker's transformation.

to twice its original length and one-half its original height. This rectangle is then cut vertically and the right half placed on top of the left to reform the unit square as shown in Fig. 15. In essence, each iteration maps the point (x,y) into (2x, y/2).

Let us now develop an arithmetic representation of the baker's transformation by writing the x and y coordinates of an initial point in binary, and then writing x to the right of the decimal in the usual order, but writing y backward to the left of the same decimal. We then typically have

$$\underbrace{\cdots 11010001}_{\leftarrow y_0} \cdot \underbrace{0011101\cdots}_{x_0 \rightarrow} \tag{40}$$

Now we observe that moving the decimal to the right gives the forward iterates of the point (x_0,y_0) while moving the decimal to the left provides backward iterates. Clearly each movement of the decimal to the right doubles x and halves y as required; less obviously, it also properly accounts for the cutting and folding. Initially, close points clearly separate exponentially for this model; moreover it may be shown to have an everywhere dense set of unstable periodic orbits. Thus this mapping mimics the stochastic zones previously discussed.

Now let us observe that on each forward iteration or rightward movement of the decimal in representation (40), the first digit to the right of the decimal determines whether the new iterate lies to the left or the right of x = 1/2. But in general, the sequence of zeroes and ones in these binary representations is as random as a coin toss. Thus quite clearly, the iterated points for the baker's transformation random walks between the

right and left sides of the unit square. Indeed, if we define an initial probability density $W_0(x)$ on the unit square, then we obtain a random walk type diffusion equation

$$W_{n+1}(x) = (1/2)[W_n(x/2) + W_n((x+1)/2)] , \qquad (41)$$

whose derivation is immediately obvious since the point x on the (n+1) iteration can only be reached from the points (x/2) and (x+1)/2 on the previous iteration. It is to be hoped that the macroscopic consequences of the stochastic zones are now becoming clearer.

THE BOUNCING BALL MODEL

A physically more realistic "random walk" system and one closer to the Chirikov Hamiltonian of the previous section is provided by the bouncing ball model. This example was originally developed by Fermi[4] and Ulam[5] as a highly simplified model of cosmic ray acceleration. Consider a ball bouncing between two infinitely heavy walls, one fixed and one oscillating as shown in Fig. 16. The ball has instantaneous speed v and the moving wall oscillates with amplitude a, period T, and instantaneous speed $V(t)$, where $V(t)$ is a sawtooth function having the maximum value V. The minimum distance between the walls is ℓ. The exact difference equations governing the motion of this system are presented in a paper[6] by Zaslavskii and Chirikov. Following Lieberman and Lichtenberg[7], we elect to consider an approximation to these

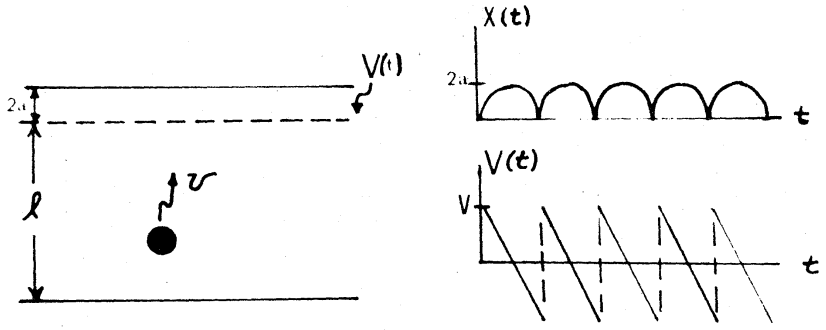

Fig. 16. Diagram of the Fermi-Ulam system used to model the acceleration of cosmic rays.

exact difference equations. The approximating equations are

$$u_{n+1} = |u_n + \psi_n - \tfrac{1}{2}| \qquad (42a)$$

$$\psi_{n+1} = \left[\psi_n + \left(\frac{M}{u_{n+1}}\right)\right] , \text{ (mod 1)} \qquad (42b)$$

where $u_n = v_n/V$, v_n is the speed of the ball just before the nth collision with the oscillating wall, $\psi_n (0 \leq \psi_n \leq 1)$ is the phase of the oscillating wall at the nth collision, and $M = (\ell/16a)$. Equation (42) is a good approximation to the exact equations of motion provided that $M \gg 1$ and $u \gg 1$; however, independent of the goodness of these approximations, Eq. (42) yields the same general type of behavior as do the much more complicated exact equations. We therefore confine our attention to Eq. (42).

Our first observation is that Eq. (42) reduces our problem to the study of a plane area-preserving mapping. However, this mapping does not exhibit everywhere exponentially separating orbits throughout the (ψ,u) plane; like the systems of the preceding two sections, this system exhibits a so-called divided phase space[3]. Indeed, taking differentials of Eq. (42), we obtain

$$\begin{aligned} du_{n+1} &= du_n + d\psi_n \,, \\ d\psi_{n+1} &= d\psi_n - \left(\frac{M}{u^2_{n+1}}\right) du_{n+1} \end{aligned} \tag{43}$$

Now for the (ψ,u) region which shall interest us in these calculations, we have $u_n \gg 1$ and $M \gg u_n$; moreover, (42a) shows that $u_n \gg 1$ varies slowly with n. Thus, let us approximate in (43) and set (M/u^2) equal to a constant, b say. Equation (43) may then be written

$$\begin{aligned} du_{n+1} &= du_n + d\psi_n \\ d\psi_{n+1} &= -b\, du_n + (1 - b) d\psi_n \,, \end{aligned} \tag{44}$$

where

$$0 < b = \frac{M}{u^2} \,. \tag{45}$$

A linear change of variables now permits us to write Eq. (44) in the form

$$d\zeta_{n+1} = \lambda\, d\zeta_n, \qquad d\eta_{n+1} = \lambda^{-1}\, d\eta_n \,, \tag{46}$$

$$\lambda = \tfrac{1}{2}(2 - b) - \tfrac{1}{2}[(2 - b)^2 - 4]^{1/2} \,. \tag{47}$$

From Eq. (47), we see that λ is real when $b > 4$ and is imaginary when $0 < b < 4$. Thus referring to Eq. (46), we see that iterates of Eq. (44) oscillate when $u > M^{1/2}/2$ and they exponentiate when

$u < M^{1/2}/2$. We thus expect stochastic behavior for the mapping of Eq. (42) in that (ψ,u)-plane region for which

$$u < \frac{M^{1/2}}{2} \tag{48}$$

and smooth curves for $u > M^{1/2}/2$. In the stochastic region, each small initial $(d\psi_0\ du_0)$ area-element grows exponentially in the ζ-direction and shrinks exponentially in the η-direction. Further, since the expanding ζ-direction has small but nonzero slope $(\Delta u/\Delta\psi) \approx -(1/b)$ for $b >> 1$, both variables u and ψ locally spread exponentially, but ψ spreads more rapidly than u.

In Fig. 17, we show a composite sketch of a typical Eq. (42)-mapping based on several computer-generated figures presented by Brahic[8] and Lieberman and Lichtenberg[7]. In Brahic's paper especially, some of the mapping pictures represent a striking form of abstract art. In Fig. 17, we note that the boundary of the stochastic behavior occurs at about the predicted value of $u = M^{1/2}/2$. For larger u-values, again as predicted, stable as well as unstable fixed points appear. By direct substitution, one easily finds that the mapping T of Eq. (42) has fixed points of T itself at $(\psi,u) = (1/2, M/k)$, where k is a positive integer, and that these fixed points are stable when $u > M^{1/2}/2$. The member of this fixed point set having the largest associated stable region, as seen in Fig. 17, lies at (1/2,M), and physically corresponds to the ball being reflected from the oscillating wall (at $\psi = 1/2$ when the moving wall instantaneously has zero speed) and then colliding again with the moving wall after the elapse of precisely one wall period. Fixed points of T^2, T^3, etc., can also be determined through increasingly long and tedious algebraic manipulations of Eq. (42).

For motion in the stochastic region where $u < M^{1/2}/2$, Lieberman and Lichtenberg[7] first establish that the relaxation times for the u and ψ motion differ widely. They then use this fact to obtain an irreversible rate equation which they validate using a computer. In Eq. (42), let us start with a precise initial (ψ_0,u_0) state (a definite state and not a rectangle $d\psi_0\ du_0$) for which $M >> u >> 1$. Then, as n increases, the sequential iterates of ψ_n will rapidly cover the whole interval $0 \lesssim \psi \lesssim 1$ in a "random" manner much before $(\Sigma|\Delta u_n|)/u_0$ becomes large. As a consequence, the fractionally small, sequential iterates Δu_n generated by Eq. (42a) will be positive or negative with about equal frequency, and u_n will perform a relatively slow "random walk" away from the initial region near u_0. Alternatively, consider an ensemble of systems with initial states spread uniformly over a small rectangle $(d\psi_0 du_0)$.

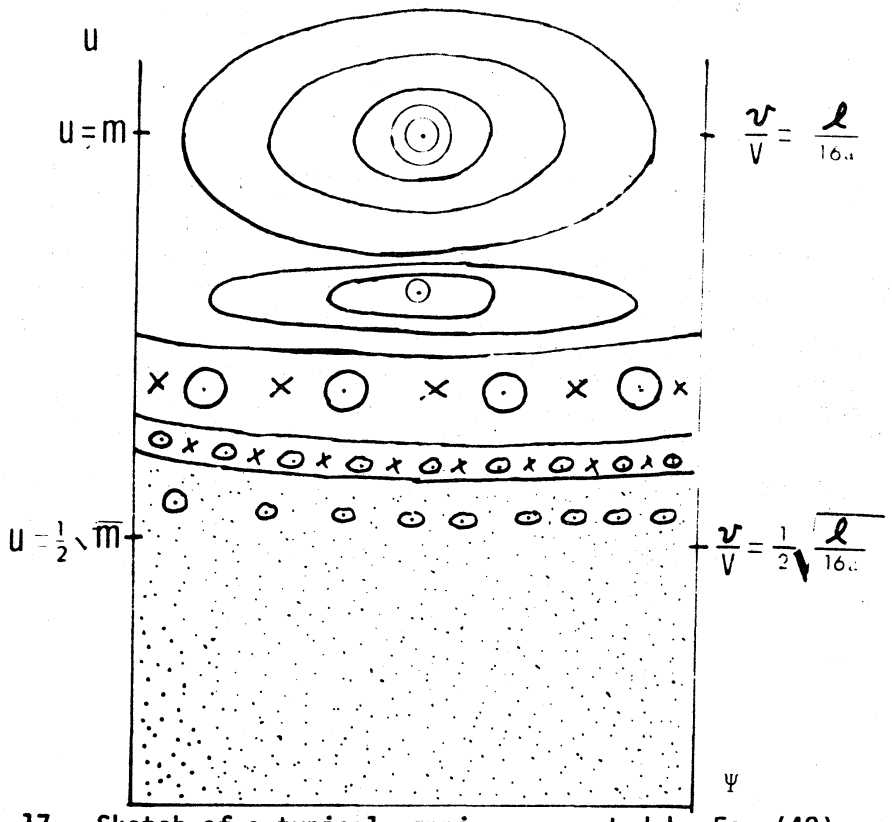

Fig. 17. Sketch of a typical mapping generated by Eq. (42).

According to the discussion following Eq. (48), the small rectangle will spread exponentially along the ζ-direction into an almost horizontal filament with $\delta\psi \sim 1$ and $(\delta u/u) << 1$. Although each small segment of this filament will continue locally to grow exponentially, macroscopically the next iteration of this filament will split into two or more new filaments, each having $\delta\psi \sim 1$. Moreover, since the original filament had $\delta\psi \sim 1$, Eq. (42a) ensures that half of the almost horizontal, new filaments lie slightly above (along the u-axis) the original filament and half slightly below. Similarly one more iteration splits each of these new filaments into a newer set, equally split above and below the original, new filament position. Thus in the ensemble, the system phases ψ "randomize" on an exponential time scale followed, on a much longer time scale, by a diffusive spread of the u-values.

On the basis of either of these arguments, one concludes that Eq. (42b) causes the fine-grained density $\int(\psi,u,n)$ to mix continually along the ψ-direction with exponential rapidity. Equation (42a) then ensures that the reduced probability distribution W(u,n) spreads along the u-direction via a much slower random walk process which is known[9] to lead to a type of diffusion equation. One therefore expects that W(u,n) satisfies the Fokker-Planck equation[9]

$$\frac{\partial W}{\partial n} = -\frac{\partial}{\partial u}(BW) + \frac{1}{2}\frac{\partial^2}{\partial u^2}(DW) \ . \qquad (49)$$

In order to verify the use of Eq. (49) for this system, B and D are calculated using Eq. (42) in the Wang-Uhlenbeck formulas[9].

The results can then be compared with the computer-calculated values for B and D. Starting from $W(u,0) = \delta(u - u_0)$, Eq. (49) predicts that the width of W should grow like $n^{1/2}$, which can also be checked against computer calculations. Finally $W(u,\infty)$ should be a constant over the stochastic region. In all cases, theory and computer experiment agree nicely. For example, in Fig. 18, adapted from Ref. 7, we show a plot of $W(u,\infty)$ versus u obtained by integrating Eq. (42) for an ensemble of systems. Here $W(u,\infty)$ is more or less constant up to the stochastic border $u = M^{1/2}/2 = 10^{3/2}/2 \simeq 16$, above which W falls off quite rapidly.

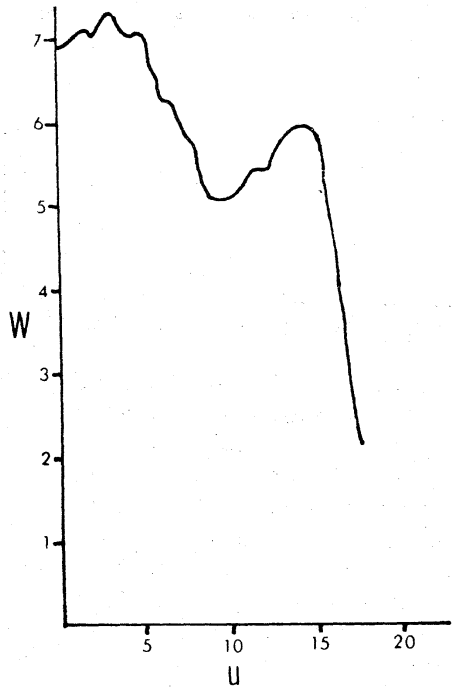

Fig. 18. A graph of the probability density $W(u,\infty)$ as a function of u. W is specified in arbitrary units.

A rigorous derivation of Eq. (49) from Eq. (42) lies in the future. Nonetheless this example and the previous one point in the direction of future progress[10] in developing rate equations for physical systems exhibiting stochastic behavior.

CONCLUDING REMARKS

Hamiltonian systems of the type $H = H_0(J) + \varepsilon V(J,\phi,\tau)$ exhibit a complete spectrum of behavior ranging from complete integrability to complete stochasticity. In this review, we have presented a pictorial, intuitive discussion of this behavior in terms of non-linear resonances and their overlap. In this view, Hamiltonian systems whose non-linear resonances have negligible (or no) over-

lap are either precisely integrable or else nearly integrable. On the other hand, Hamiltonian systems whose non-linear resonances increasingly overlap as some parameter is varied exhibit chaotic orbits in increasingly large phase space regions. Indeed example systems[11] have recently been discovered in which one can observe the full transition from complete integrability to complete stochasticity.

In the latter sections of this review, we have discussed example systems which provide some insight into the macroscopic consequences caused by the chaotic orbits of the underlying microscopic dynamics. In a not too remote future, one anticipates that all of equilibrium and non-equilibrium statistical mechanics will be rigorously derivable from basic dynamics, either classical or quantum. But already, practical applications are being developed in astronomy, biology, chemistry and in many areas of physics, and these developments will likely continue into the distant future.

Many people have been and are participating in this work, and the author apologizes to those whose contributions are not directly referenced here. Perhaps it suffices merely to publically state that the present author's meager understanding of this subject has been derived from a superior understanding possessed by a host of non-linear scientists so large that even a partial listing would be tediously long.

REFERENCES

1. One may find further references to the now extensive literature in J. Ford, Fundamental Problems in Statistical Mechanics, Vol. 3, edited by E. D. G. Cohen (North-Holland, Amsterdam, 1975); A. S. Wightman, Statistical Mechanics at the Turn of the Decade, edited by E. D. G. Cohen (North-Holland, Amsterdam, 1968); J. Moser, Mem. Am. Math. Soc., #81 (1968); G. Contopoulos, Bull. Astron. 2, 223 (1967); N. Saito, N. Ooyama, Y. Aizawa, and H. Hirooka, Prog. Theor. Phys. Suppl. 45, 209 (1970); G. M. Zaslavsky and B. V. Chirikov, Soviet Phys. Uspekhi 14, 549 (1972).
2. V. I. Arnold and A. Avez, Ergodic Problems of Classical Mechanics (Benjamin, New York, 1968).
3. B. V. Chirikov, Phys. Reports (to appear in 1978). The present author is appreciative for being allowed to review this paper prior to publication.
4. E. Fermi, Phys. Rev. 75, 1169 (1949).
5. S. M. Ulam, Proceedings of the Fourth Berkeley Symposium on Mathematical Statistics and Probabilities, Vol. 3 (Univ. California Press, Berkeley, 1961).
6. G. M. Zaslavsky and B. V. Chirkov, Soviet Phys. Doklady, 9, 989 (1965).
7. M. A. Lieberman and A. J. Lichtenberg, Phys. Rev. A5, 1852 (1972).
8. A. Brahic, Astron. Astrophys. 12, 98 (1971).

9. M. C. Wang and G. E. Uhlenbeck, Rev. Mod. Phys. 17, 323 (1945).
10. A. N. Kaufman, Phys. Rev. Lett. 27, 376 (1971).
11. G. Benettin and J. M. Strelcyn, Phys. Rev. A (to appear in 1978).